Article

Improvement of Oral Bioavailability of Pyrazolo-Pyridone Inhibitors of the Interaction of DCN1/2 and UBE2M

Ho Shin Kim, Jared T. Hammill, Daniel C. Scott, Yizhe Chen, Amy L. Rice, William Pistel, Bhuvanesh Singh, Brenda A. Schulman, and R. Kiplin Guy*

Read Online

ACCESS | 📊 Metrics & More | 📰 Article Recommendations | 🆂🆘 Supporting Information

ABSTRACT: The cullin-RING ubiquitin ligases (CRLs) are ubiquitin E3 enzymes that play a key role in controlling proteasomal degradation and are activated by neddylation. We previously reported inhibitors that target CRL activation by disrupting the interaction of defective in cullin neddylation 1 (DCN1), a CRL neddylation co-E3, and UBE2M, a neddylation E2. Our first-generation inhibitors possessed poor oral bioavailability and fairly rapid clearance that hindered the study of acute inhibition of DCN-controlled CRL activity in vivo. Herein, we report studies to improve the pharmacokinetic performance of the pyrazolo-pyridone inhibitors. The current best inhibitor, **40**, inhibits the interaction of DCN1 and UBE2M, blocks NEDD8

transfer in biochemical assays, thermally stabilizes cellular DCN1, and inhibits anchorage-independent growth in a DCN1 amplified squamous cell carcinoma cell line. Additionally, we demonstrate that a single oral 50 mg/kg dose sustains plasma exposures above the biochemical IC_{90} for 24 h in mice.
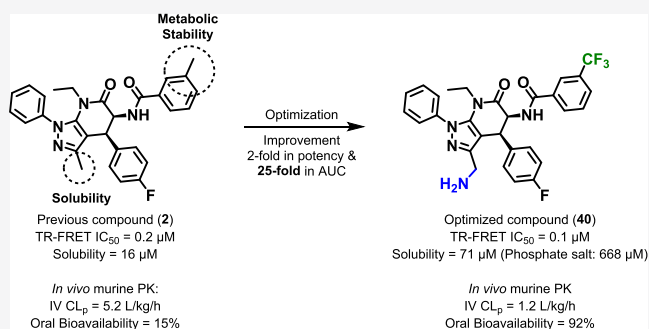
INTRODUCTION

Neddylation is a post-translational modification that conjugates the neural precursor cell expressed, developmentally down-regulated 8 (NEDD8) protein to protein substrates. Neddylation occurs through a three-step enzymatic cascade. First, NEDD8 is conjugated to a cysteine of the E1 in an ATP-dependent manner. Next, a transthioesterification reaction transfers the NEDD8 to a cysteine on the E2. Finally, NEDD8's C-terminus is ligated to the γ-amino group of a lysine side chain on the target protein forming an isopeptide bond. The best-known neddylation substrates are the cullins, which upon neddylation join a multiprotein complex to form cullin-RING ubiquitin E3 ligases (CRLs). The CRLs are the largest class of ubiquitin E3 ligases that control ubiquitination of many proteins. Ubiquitination is a closely related post-translational modification pathway that regulates many biological processes, including proteosomal degradation of targets. CRL dysfunction is implicated in a number of human diseases, including cancer.[1−3]

Extensive drug discovery efforts have targeted the CRLs and the associated proteasomal protein degradation machinery.[4−11] The neddylation pathway can be completely inhibited by the E1 inhibitor pevonedistat (MLN4924), which is currently being investigated in multiple oncology clinical trials.[12] NEDD8 is removed from cullins by the COP9 signalosome (CSN). Inhibitors of the CSN have also been described and display promising antitumor activity in animal models.[13] While

complete ablation of neddylation appears to be clinically efficacious,[14] global inhibition of neddylation may limit its therapeutic index. In an effort to maintain efficacy and reduce toxicity, we sought more subtle ways to regulate the neddylation pathway.[15]

Defective in cullin neddylation 1 (DCN1) is also known as DCUN1D1, DCNL1, or squamous cell carcinoma-related oncogene (SCCRO); we use "DCN1" hereafter. DCN1 acts as a co-E3 together with RBX1 to stimulate the transfer of NEDD8 from its E2 (UBE2M) to the cullin proteins, regulating CRL stability, intracellular localization, and function.[16] The neddylation and ubiquitination pathways are complex dynamic processes. Thus, the development of efficacious chemical probes, which permit acute and selective inhibition of DCN-mediated CRL activity, has the potential to help unravel the mechanisms regulating key cellular signaling networks and driving disease progression. In humans, the DCN family contains five isoforms. The best characterized DCN isoforms are DCN1 and DCN2, which are highly homologous and may be redundant in mammals.[17−24] They also have the strongest
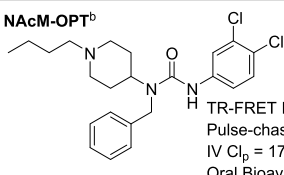
Table 1. SAR and SPR of Hinge Pocket[a,b]

NAcM-OPT[b]

TR-FRET IC$_{50}$ = 0.08 μM
Pulse-chase IC$_{50}$ = 0.17 μM
IV Cl$_p$ = 17 L/hr/kg
Oral Bioavailability = 88%

No	R	IC$_{50}$ (μM) (TR-FRET)	CLint' (ml/min/kg) (mouse)	Avg. Sol. (μM) (Kinetic)	No	R	IC$_{50}$ (μM) (TR-FRET)
1	phenyl	1.32 ± 0.08	N.D.	N.D.	9	3,4-dichlorophenyl	3.23 ± 0.37
2	m-methylphenyl	0.20 ± 0.04	44.9 ± 3.7	16.6 ± 0.6	10	m-aminophenyl	4.32 ± 0.29
3	m-chlorophenyl	0.64 ± 0.04	<13.7	5.2 ± 2.1	11	2-methylpyridinyl	>15
4	m-CF$_3$-phenyl	0.32 ± 0.03	<13.7	11.1 ± 5.0	12	benzoxazole	>15
5	m-CN-phenyl	2.17 ± 0.24	N.D.	N.D.	13	cyclohexyl	>15
6	m-tert-butylphenyl	2.06 ± 0.16	N.D.	N.D.	14	benzyl	>15
7	2-methylthiazolyl	0.52 ± 0.08	35.1 ± 2.9	8.5 ± 1.4	15	HN-m-CF$_3$-phenyl	>15
8	2-CF$_3$-thiazolyl	0.69 ± 0.11	31.5 ± 2.6	3.7 ± 0.9			

[a]IC$_{50}$ values were generated using our time-resolved fluorescence energy transfer (TR-FRET) binding assay and are represented as the mean of three replicates with errors reported as the standard deviation. [b]Chemical structure and key data for NAcM-OPT.
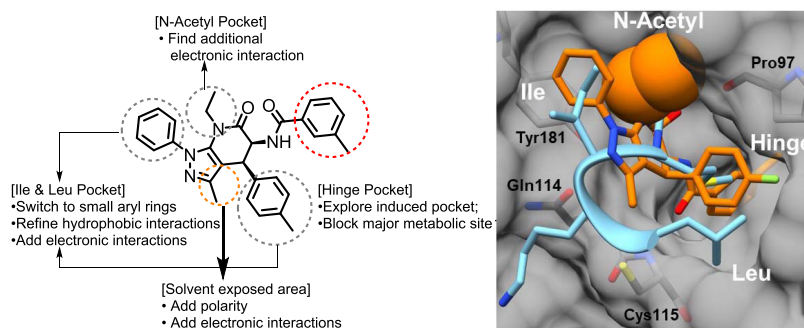

Figure 1. Design strategy and X-ray co-structure overlay of compound **2**:DCN1 (PDB 6P5V) and UBE2M:DCN1 (PDB 3TDU), highlighting the key residues for interaction and regions targeted for optimization. The key N-terminal residues of UBE2M that control binding to DCN1 are represented in cyan, compound **2** in orange, and the DCN1 protein as surface in gray with key residues shown as sticks.

associations with disease progression, especially squamous cell carinomas.[17,20,23,25,26]

We and others have discovered potent and selective inhibitors of the DCN1/2-UBE2M protein interaction.[27−33] These inhibitors all bind to and thermally stabilize DCN1 in cells and selectively reduce the steady-state levels of cullin neddylation in a variety of cell lines including HCC95, CAL33, KYSE70, H2170, SK-MES-1, and MGC-803 cells.[27−33] As a class, the DCN1/2 inhibitors have less

pronounced effects on CRL-based proteasomal degradation than global neddylation inhibitors targeting the NEDD8 E1, like MLN4924. This difference arises because the DCN1/2 inhibitors are isoform-selective and only partially inhibit cullin neddylation. Although the current DCN1 inhibitors are useful tools for in vitro studies, only the piperidinyl series, represented by NAcM-OPT (Table 1), are reasonably orally bioavailable in the mouse.[27] However, even high doses of NAcM-OPT (200

Scheme 1. Synthesis of Pyrazole Methyl-Modified DCN1 Inhibitors
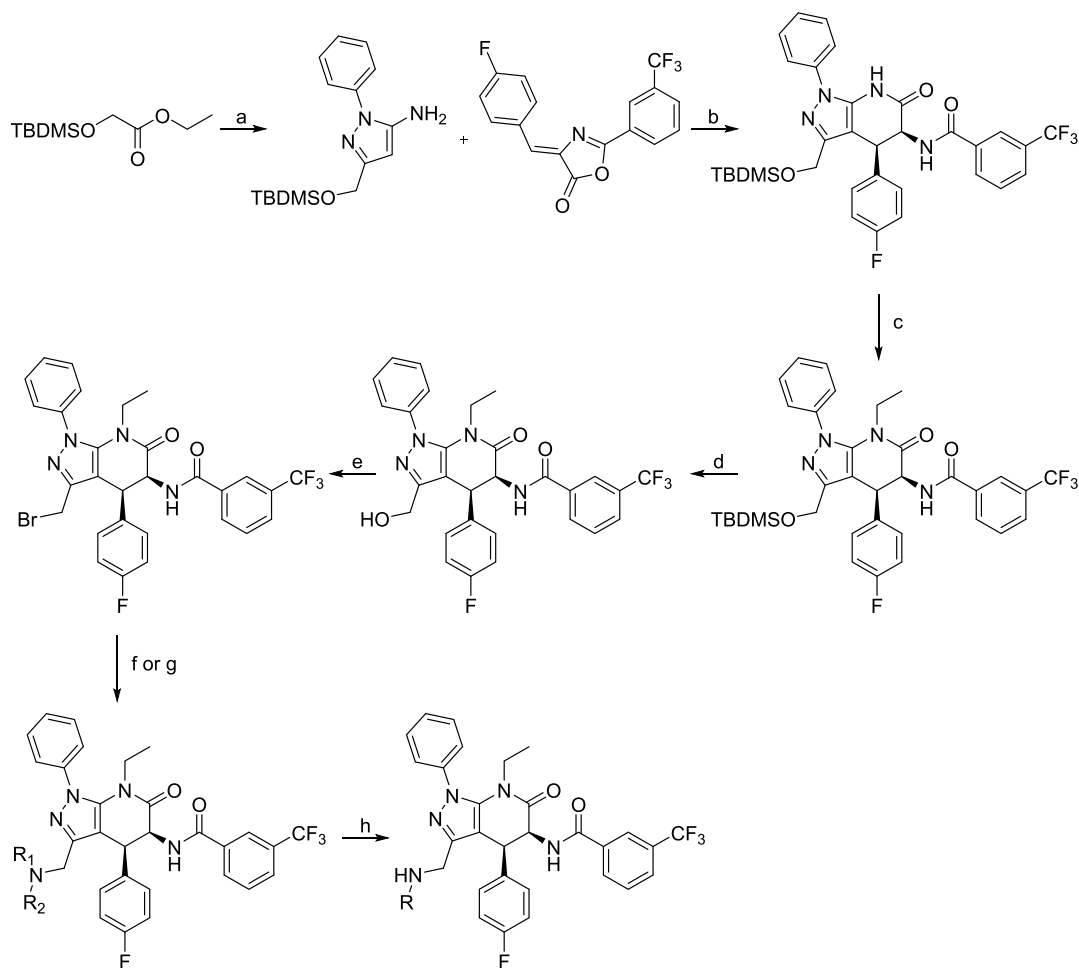
mg/kg, BID) do not continuously maintain plasma concentrations at or above its cellular IC_{90}.[27]

We recently disclosed the pyrazolo-pyridones, a class of DCN1 inhibitors designed to address several limitations of NAcM-OPT including: (1) failure to access the N-acetyl subpocket in the targeted binding pocket that controls the binding of the native substrate; (2) a minimal three-dimensional character, limiting efficient access of the available binding subpockets; and (3) the moderate murine half-life and C_{max} that drive the poor pharmacokinetic profile.[33] Our initial work focused on addressing the first two points, identifying the minimum pharmacophore for this class, and defining the structural drivers of potency for binding to DCN1. Briefly, these studies yielded compound **2**, which was 25-fold more potent than the original HTS hit compound. Compound **2** design was based on insights derived from overlaying the X-ray co-structures of the HTS hit:DCN1 (PDB 6P5W), UBE2M^{NAc}:DCN1 (PDB 3TDU), and NAcM-OPT:DCN1 (PDB 5V86).

The previous SAR studies revealed four critical components: (1) a strong preference for the cis stereochemistry of the pyrazolo-pyridones; (2) a preference for small alkyl substitution of the pyridone nitrogen; (3) wide flexibility with respect to the identity of substituents fitting either Ile or Leu pocket, but the potential for metabolic degradation; and (4) very restrictive requirements for the substituent targeting the hinge pocket (Figure 1). The best lead compound arising from those studies,

compound **2**, is potent and selective but only moderately soluble and stable in microsomal models. Compound **2** does not address the key liability of NAcM-OPT—the poor pharmacokinetics hindering the use for modeling in vivo. To address this issue, we embarked on a second medicinal chemistry campaign to develop chemical probes of pyrazolo-pyridone class useful for in vivo studies.

Herein, we summarize the key learnings from this campaign in which we prepared and analyzed over 150 new analogues designed based on the hypotheses generated by combining empirically derived SAR/SPR from earlier studies with examination of X-ray co-structures. New analogues were tested for their ability to inhibit the target protein interaction using our previously reported TR-FRET assay based on the TR-FRET signal between a biotinylated DCN1 protein, recognized by Terbium-linked streptavidin, and the helical stapled peptide derived from N-terminally acetylated UBE2M harboring a C-terminal AlexaFluor 488.[29] Active and potent compounds were evaluated for biochemical inhibition of neddylation in a reconstituted pathway cascade, cellular target engagement, and inhibition of anchorage-independent growth in a DCN1 amplified cell line (HCC95). In parallel, active compounds were tested to evaluate the solubility and stability to incubation with liver microsomes. Select molecules were subjected to pharmacokinetic studies in mice. Ultimately, these studies identified compound **40**, for which a single 50 mg/kg oral dose affords continuous murine plasma exposure above its bio-

Scheme 2. Parallel Synthesis of Analogues Targeting the Hinge Pocket
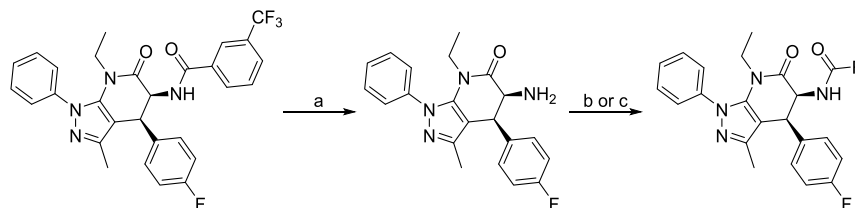
chemical IC$_{90}$ for at least 24 h. Compound **40** was also slightly (2-fold) more potent than compound **2** at inhibiting the DCN1-UBE2M interaction, thermally stabilizes DCN1 in cells, and inhibits anchorage-independent growth of transformed cells.

■ RESULTS

Design and Synthesis. The pyrazolo-pyridones were discovered during our initial high-throughput screening campaign (HTS)[29] and optimized for potency to give compound **2**.[33] Relative to the first class of inhibitors reported by our group, as exemplified by NAcM-OPT[33] the pyrazolo-pyridones possess a high degree of three-dimensional structure that affords opportunities for increased binding potency, target selectivity, and improved solubility. The structure-guided optimization that afforded **2** defined four key subpockets within the binding site: Ile, Leu, N-acetyl, and hinge pockets (Figure 1). The most important learning from these studies was that ethyl substitution of the pyridone nitrogen could induce tighter binding by enhanced hydrophobic packing compared to the indirect water-mediated binding mode seen with unsubstituted pyridones. Although compound **2** is potent and selective, it is also poorly water-soluble and readily metabolized leading to poor bioavailability. We embarked on the second medicinal chemistry campaign to improve the bioavailability of compound **2**.

Our overall goal was to achieve a 10-fold improvement in plasma exposure (AUC) while maintaining or improving potency. Thus, we set out to: (1) reduce in vivo clearance by suppressing oxidative metabolism; (2) improve aqueous solubility and maximal plasma exposure by reducing hydrophobicity and crystallinity; (3) refine the pharmacophore by revisiting favored substituents for the Ile, Leu, and Hinge pockets within the context of the cis-ethyl pyridone; and (4) expand the range of N-acetyl pocket substituents with hydrophilic substitutions that may form beneficial electrostatic or hydrogen-bonding interactions within the N-acetyl pocket.

New compounds were synthesized using a modification of our previously reported three-step procedure (Scheme 1)[33] consisting of: preparation of an oxazolone intermediate,[34] pyrazolo-pyridone ring formation,[35] and substitution using alkylation or acylation. Formation of the core pyrazolo-pyridone ring afforded a separable mixture of cis- and trans- diastereomers, which were assigned based on the $^3J_{H-H}$ vicinal proton–proton coupling for the C4 or C5 protons of pyrazolo-pyridone ring (cis = 7–8 Hz, trans = 9–11 Hz). Focused derivatization of the pyrazole methyl began with displacement of the ethoxy group of silyl-protected ethyl glycolate with acetonitrile. Subsequent reaction with various hydrazines afforded the key 5-amino-3-silyl-protected hydroxyl pyrazole intermediates. Cyclization of the amino pyrazole with an oxazolone, ethylation of the pyridone, and silyl deprotection produced free hydroxylated compounds, generally in moderate yields. The introduction of structural diversity on the solvent-exposed methyl pyrazole was

accomplished via either Appel reaction and substitution or Gabriel synthesis. This route, while efficient, was not amenable to rapid diversification of the hinge pocket. For this purpose, we modified the synthetic route to include amide hydrolysis, followed by either acylation with an acid chloride/anhydride or EDCI-mediated amide coupling (Scheme 2). Unless otherwise specified, all compounds were purified using flash column chromatography and their purity (>95%) and identity were established by liquid chromatography, ^{1}H NMR, and HRMS analyses. Key analogues were further characterized by 13C NMR.

Reagents and conditions: (a) (i) CH$_3$CN, n-BuLi, ethyl glycolate, tetrahydrofuran (THF), −78 °C to room temperature (rt), 2h, (ii) phenyl hydrazine, chlorobenzene, reflux, 16 h; (b) chlorobenzene, 170 °C, in pressure vessel, 16 h; (c) EtBr, Cs$_2$CO$_3$, dimethylformamide (DMF), rt, 16 h; (d) HCl, CH$_3$CN, rt, 16 h; (e) CBr$_4$, PPh$_3$, dichloromethane (DCM), 0 °C to rt, 16 h; (f) R$_1$R$_2$N, N,N-diisopropylethylamine (DIPEA), DCM, 0 °C to rt, 16 h; (g) (i) phthalimide, K$_2$CO$_3$, DMF, rt, 16 h, (ii) hydrazine monohydrate, DCM, 0 °C to rt, 16 h; (h) Ac$_2$O or MsCl or R-COCl, DIPEA, DCM, 0 °C to rt, 1 h.

Reagents and conditions: (a) c-HCl, 1,4-dioxane, 85−90 °C, 16 h; (b) R-COOH, EDCI·HCl, DCM, rt, 16 h; (c) R-COCl, DIPEA, DCM, rt, 16 h.

Structure−Activity and Structure−Property Relationships. In the course of this study, we designed, prepared, and tested over 150 analogues. To provide a clearer narrative, we show in the main text only critical compounds illustrating the key structural drivers for potency (structure−activity relationships, SAR); permeability, solubility, and log D (structure−property relationships, SPR); and metabolic and toxic liabilities. Complete SAR and SPR tables, containing all compounds made and tested, can be found in the Supporting Information.
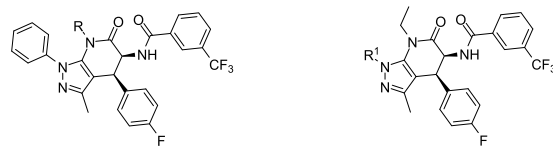
We began the campaign by validating the hypothesis that previously observed structural drivers of potency in the absence of pyridone substitution are maintained with a substituted pyridone.[33] This was done to ensure that there were no nonadditive interactions between the N-ethyl and other substituents that dramatically shifted SAR.

First, we sought to confirm the importance of the relative stereochemistry of the pyrazolo-pyridone ring. Surprisingly, some trans analogues, which in the absence of pyridone substitution were universally inactive (>15 μM), exhibited moderate activity. In some cases, they were even as potent as their cis counterparts. However, not all trans analogues exhibited activity (Table S10). Therefore, we maintained focus on the cis diastereomers for all future work and to enable better comparison to legacy data.

Next, we sought to confirm the SAR about the hinge region. Similar to the unsubstituted pyridone SAR,[33] substituents targeting the hinge pocket maintained structural requirements, requiring a small hydrophobic substitution such as a meta-methyl group for maximal potency. Removing all substitution

from the aryl ring (**1**) decreased the potency 6-fold. Replacement of the methyl group with roughly isosteric electron-withdrawing groups was well tolerated (CF3 (**4**), Br (**48**), I (**49**), Table S1). Significantly smaller or larger substituents decreased potency. Smaller heterocyclic replacements of the phenyl ring were tolerated in some, but not all cases (**7**, **8**, Table S2), with no clear trends beyond the steric fit. Polar substituents (**10**, **11**, **71**, **72**; Tables S1 and S2) were not favored. Adding fluorine atoms was generally tolerated, but decreased potency relative to nonfluorinated analogues (Tables 1, 2 vs 4

Table 2. SAR of *N*-Acetyl Pocket and IIe Pocket[a]

No	R	IC$_{50}$ (μM) (TR-FRET)	No	R^1	IC$_{50}$ (μM) (TR-FRET)
4	(ethyl)	0.32 ± 0.03	22	(propyl)	0.54 ± 0.05
16	(propyl)	1.93 ± 0.07	23	F$_3$C-(CH$_2$)	2.43 ± 0.25
17	(cyclopropylmethyl)	1.24 ± 0.11	24	(cyclopropyl)	0.50 ± 0.07
18	(methoxyethyl)	1.19 ± 0.11	25	(o-tolyl)	0.51 ± 0.03
19	HO-(ethyl)	0.34 ± 0.03	26	(o-CF$_3$-phenyl)	1.91 ± 0.13
20	H$_2$N-(ethyl)	8.41 ± 2.59			
21	NC-(ethyl)	>15			

[a]IC$_{50}$ values were generated using our TR-FRET binding assay and are represented as the mean of three replicates with errors reported as the standard deviation.

and S1). Any significant increase in steric bulk was poorly tolerated. Bicyclic replacement (**12**) or mimicking the optimized hinge pocket of NAcM-OPT (**9**) significantly reduced potency. Aliphatic substitution (**13**), elongation of the linker (**14**), or isosteric replacement of the linker (**15**, Table S2) were not tolerated. Throughout this study, analogues containing ethyl substitution of the pyridone were universally more potent than their unsubstituted counterparts, consistent with the key SAR findings of our previous publication.[33] Clearly, there remains a strict steric requirement for this substituent that does not permit size modifications without loss of potency. Taken together, these two preliminary studies confirmed overall maintenance of the previously defined SAR.

The major liabilities identified during the first round of optimization were poor aqueous solubility and moderate oxidative metabolic stability.[33] To assess if the microsomal models were accurately predicting in vivo clearance, we tested compound **2** in single-dose intravenous (iv) and oral pharmacokinetic (PK) studies (Figures 2 and S6). We did not observe any adverse reactions or compound-related side effects within 48 h after dosing. Compound **2** was poorly oral bioavailable (15%) and rapidly cleared both in vitro and in vivo (intrinsic MLM CL$_{int}$ = 44.9 mL/min/kg, predicted in vivo hepatic CL = 32.7 mL/min/kg, murine plasma CL$_{IV}$ = 86.5 mL/
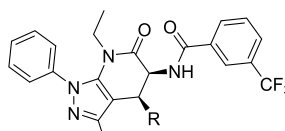
min/kg, 5.2 L/h/kg). Maximal plasma exposure (C$_{max}$ = 0.36 μM) at 50 mg/kg oral dose was also limited. Overall, there was a good correlation between predicted clearance from microsomal models and observed clearance. To guide the design of metabolically stable analogues, we conducted metabolite identification (Met-ID) studies for compound **2** after microsomal incubation, revealing that oxidation of the aryl amide substituent targeting the hinge pocket was the major route of metabolism. Electronically and physically deactivating the site of metabolism by introducing halogenated substituents significantly decreased the rate of metabolic oxidation (**3**, **4**, Table 1 and Figure 2), while electron-donating substituents made the compounds more susceptible to oxidative metabolism (OCH3, **50**, Table S1). Since the *meta*-CF3 phenyl ring afforded the best combination of potency, solubility, and oxidative metabolic stability (**4**, Table 1 and Figure 2), we anchored further studies upon that substituent and began to explore the *N*-acetyl pocket.

Our initial SAR study[33] included a systematic exploration of substituents targeting the *N*-acetyl pocket. That study revealed that ethyl substitution of the pyridone most effectively occupied the *N*-acetyl binding pocket on DCN1 and improved potency 5- to 10-fold, relative to nonethylated analogues. Previous biochemical and crystallography studies have shown that occupancy of this pocket on DCN1 by the native acetylated N-terminus of UBE2M is critical for the protein interaction and stabilized by both hydrophobic fulfillment of the pocket and hydrogen bonding between the N-terminal amide of UBE2M and two key residues on DCN1: the donor hydroxyl of Tyr181 and acceptor amide backbone of Pro97 (PDB 3TDU).[25]

Therefore, we revisited the *N*-acetyl pocket with a focus on the introduction of substituents including hydrogen-bond donors and acceptors. While we surveyed almost 20 substituents (Table S3), only the ethyl hydroxy (**19**) was comparably potent to the ethyl analogue (**4**). Other groups including the lipophilic F (**83**), CN (**21**), and hydrophilic NH2 (**20**) were not tolerated (Tables 2 and S3). Although the hydroxyl (**19**) is polar and retains metabolic stability, it did not improve aqueous solubility. The combination of data suggests a strict steric requirement, which is further supported by the analysis of the X-ray co-crystal structure (Figure 1). A brief survey of substituents targeting the Ile pocket revealed that replacement of the phenyl ring with a small aliphatic group (**22**, **24**) was well tolerated in terms of potency but led to a reduction in metabolic stability (Table S4). Fluorinated substituents, meant to suppress *n*-dealkylation, were not tolerated (**23**, **26**, Table 2).

Next, we focused on further exploration of substituents targeting the Leu subpocket. We explored replacing one of the three aryl rings that cause the compounds high log D[36] with heterocycles designed to improve water solubility. Some heterocyclic analogues retained potency (**27–29**, Table 3). Among these, placing a sulfur atom at the 3-position proved critical for potency (**27–29**). However, placement of heteroatoms at the 2-position led to a 5-fold drop in potency (Table S5). Within the subset of active heterocycles, incorporation of a methyl group at either the 2- or 3-position was well tolerated (**28**, Table S5). Unfortunately, these heterocycles did not improve either solubility or microsomal stability.

We turned to a wider exploration of other substituents that might improve either solubility or metabolic stability. Fluorination at the para-position of the phenyl ring (**4**) proved optimal, and larger substituents reduced potency (vs **31**). Consistent with previous studies,[33] the presence of a *para*-F preserved the activity of the pyridine rings (**33**). However, the *para*-
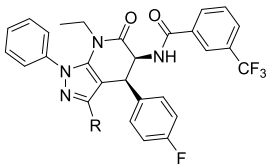
Table 3. SAR and SPR of Leu Pocket[a]

No	R	IC_{50} (µM) (TR-FRET)	CLint' (ml/min/kg) (mouse)	Avg. Sol. (µM) (Kinetic)
27	(thiophene)	0.70 ± 0.02	50.7 ± 4.4	17.3 ± 1.0
28	(methylthiophene)	0.55 ± 0.02	521 ± 2.9	N.D.
29	(isothiazole)	0.40 ± 0.02	87.8 ± 4.2	12.6 ± 0.9
30	(thiazole)	1.98 ± 0.02	N.D.	N.D.
4	(4-fluorophenyl)	0.32 ± 0.03	<13.7	16.6 ± 0.6
31	(4-bromophenyl)	0.96 ± 0.06	N.D.	N.D.
32	(benzyl)	0.74 ± 0.08	N.D.	N.D.
33	(fluoropyridine)	0.24 ± 0.03	<10.0	12.5 ± 2.5
34	(methyl-fluorophenyl)	1.27 ± 0.10	N.D.	N.D.
35	(nitro-fluorophenyl)	0.31 ± 0.06	<10.0	4.9 ± 1.4
36	(EtOOC-fluorophenyl)	>15	N.D.	N.D.

[a]IC_{50} values were generated using our TR-FRET binding assay and are represented as the mean of three replicates with errors reported as the standard deviation.

fluoropyridine analogue was not significantly more soluble than the thiophene. Other substituents at the meta-position reduced potency except the nitro group (**35**). Halogenation at ortho-position was well tolerated (Tables 3, S5 and S6). Finally, we explored the effect of increasing total rotatable bonds while reaching deeper into the Leu subpocket using the benzyl replacement for phenyl. The benzyl reduced potency 2-fold compared to its *para*-fluorophenyl analogues (**4**, **32**, Table 3).

While metabolic stability was greatly improved by fixing the *meta*-CF3 phenyl as the substituent fulfilling the hinge pocket, this modification increased compound lipophilicity ($C\log P$ **4** = 5.26) and decreased solubility. Thus, we sought to introduce a polar ionizable group that could decrease the lipophilicity and

improve aqueous solubility. Based on X-ray co-crystallography analysis (Figure 1, PDB 6P5V, 3TDU), we hypothesized that the pyrazole methyl was pointing to solvent and would be tolerant of such modifications. Indeed, the introduction of polar substituents at this position increased solubility and modestly improved potency (2- to 4-fold). Even larger substituents with longer chains (**46**, Table 4) were tolerated here. However, if substantial steric demand is introduced too close to the interior of the binding pocket, it can substantially reduce potency (**38** vs **46**, Table 4). Oxidation of the methyl to the carboxylic acid reduces potency 3-fold (**39**, Table 4). Compared to the hydroxyl

Table 4. SAR and SPR of New Pocket[a,b]

No	R	IC_{50} (µM) (TR-FRET)	CLint' (ml/min/kg) (mouse)	Avg. Sol. (µM) (Kinetic)
4	(methyl)	0.32 ± 0.03	<13.7	11.1 ± 5.0
37	HO-	0.17 ± 0.01	<13.7	7.8 ± 1.1
38	TBDMSO-	4.13 ± 0.32	N.D.	N.D.
39	HO-C(O)-	0.88 ± 0.23	N.D.	N.D.
40	H_2N-	0.10 ± 0.01	<10.0	71.0 ± 3.7
40a[b]	H_2N-	0.06 ± 0.01	N.D.	N.D.
40b[b]	H_2N-	10 ± 6	N.D.	N.D.
41	(piperidine)	0.07 ± 0.01	68.0 ± 7.9	5.3 ± 0.9
42	(methylpiperazine)	0.07 ± 0.01	14.6 ± 3.3	25.0 ± 0.9
43	(morpholine)	0.10 ± 0.01	183 ± 9.2	5.1 ± 2.4
44	(acetamide)	0.09 ± 0.02	<10.0	44.5 ± 11.7
45	(vinylsulfonamide)	0.07 ± 0.01	18.8 ± 1.8	3.5 ± 0.4
46	BocHN-	0.10 ± 0.01	N.D.	N.D.

[a]IC_{50} values were generated using our TR-FRET binding assay and are represented as the mean of three replicates with errors reported as the standard deviation. [b]Compounds **40a** (faster eluting) and **40b** (slower eluting) are the pure enantiomers of **40**, which were separated by chiral SFC.
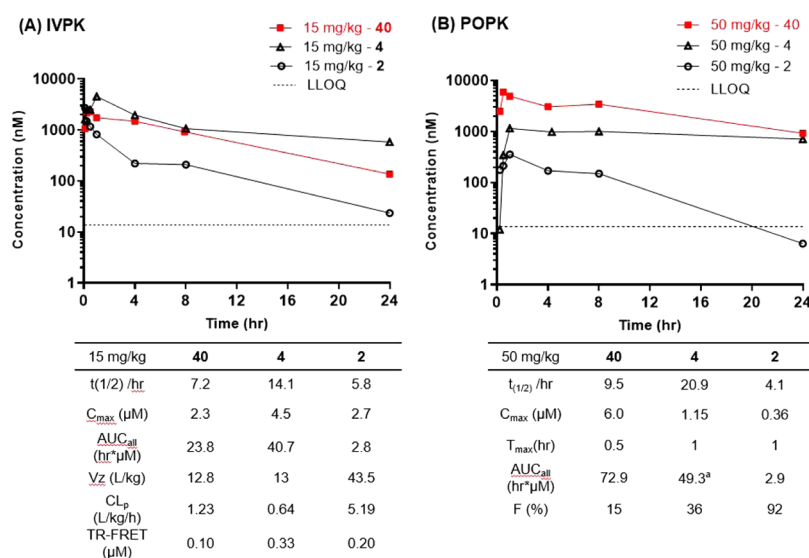
15 mg/kg	40	4	2
$t_{1/2}$ /hr	7.2	14.1	5.8
C_{max} (μM)	2.3	4.5	2.7
AUC_{all} (hr*μM)	23.8	40.7	2.8
V_z (L/kg)	12.8	13	43.5
CL_p (L/kg/h)	1.23	0.64	5.19
TR-FRET (μM)	0.10	0.33	0.20

50 mg/kg	40	4	2
$t_{1/2}$ /hr	9.5	20.9	4.1
C_{max} (μM)	6.0	1.15	0.36
T_{max}(hr)	0.5	1	1
AUC_{all} (hr*μM)	72.9	49.3[a]	2.9
F (%)	15	36	92

Figure 2. Pharmacokinetic profiling of compounds **2**, **4**, and **40**. (A) Time course of the drug plasma concentration over 24 h resulting from single-dose intravenous administration of compounds at 15 mg/kg. (B) Time course of the drug plasma concentration over 24 h resulting from single oral dose of compounds at 50 mg/kg. [a]Calculated up to 96 h time point (not fully cleared at that time). Any values of concentration below LLOQ (dotted line) were reported as half LLOQ.

analogue (**37**), the amino (**40**) or substituted amino compounds (**41–46**, **103–123**, Tables S7–S9) showed equivalent or slightly better potency (ca. 2-fold) regardless of basicity. Of the substitutions studied, primary amine **40** had the best balance of properties including good potency (100 nM), good aqueous solubility (71 μM), and excellent oxidative metabolic stability (MLM Clint <10 mL/(min kg)). The enantiomers of compound **40** were separated to ca. 99% enantiomeric excess (ee) by chiral SFC using an IG column. The faster eluting enantiomer (**40a**) was more potent (IC_{50} = 0.06 μM) than the slower eluting enantiomer (**40b**; IC_{50} = 10 μM). All further modification of the primary amine compromised microsomal stability and/or solubility (Tables S7–S9). To further improve water solubility, we prepared both the phosphate and hydrochloride salts. Both salts significantly improved solubility with the phosphate salt affording a 10-fold boost in solubility (668 μM).

To test our hypothesis that murine exposure could be improved by mitigating oxidative metabolism and increasing solubility, we selected three compounds (**2**, **4**, **40**) for murine PK modeling (Figure 2). Each compound was dosed independently by intravenous and oral routes after being formulated in EtOH/PG/PEG/PBS (10/10/40/39; v/v/v/v; pH = 7.4) and 1% (w/v) 2-hydroxy-β-cyclodextrin. As briefly discussed above, a single oral 50 mg/kg dose of **2** afforded low overall plasma exposure (50 mg/kg PO, AUC = 2.9 h·μM, C_{max} = 0.36 μM) and poor oral bioavailability (15%). We hypothesized that the low exposure and bioavailability were driven by its poor water solubility (16 μM) and fast oxidative metabolism (plasma Cl_{IV} = 5.2 L/(kg h)).

Replacement of the toluyl ring targeting the hinge pocket (**2**) with the *m*-CF$_3$ phenyl (**4**) significantly improved in vivo murine clearance (plasma Cl_{IV} = 0.64 L/(kg h); Figure 2). However, the oral plasma exposure of compound **4** (50 mg/kg PO, AUC = 23.8 h·μM, C_{max} = 1.15 μM) and oral bioavailability (36%) remained relatively low. This supported the hypothesis that clearance is predominantly driven by oxidative metabolism and strongly suggested that poor absorption driven by its low solubility (11 μM, Table 1) was also playing a role. Adding the

methylamine substitution to the pyrazole ring in this background (**40**) greatly improved total plasma exposure (50 mg/kg PO, AUC = 72.9 h·μM C_{max} = 6.0 μM), dramatically enhanced oral bioavailability (92%), and maintained minimal clearance (plasma Cl_{IV} = 1.2 L/(kg h)) (Figure 2). Compound **40** was also well tolerated at these doses with no significant changes observed in clinical chemistry, hematology, or signs monitored during a functional observational battery (Tables S16 and S17, Figures S9 and S10). These experiments established an in vitro–in vivo correlation (IVIVC) for the series between microsomal stability models, solubility, and in vivo bioavailability. This allows use of in vitro models to rapidly triage and prioritize new molecules for in vivo testing in the future (Figures 2 and S6–S8).

Biochemical and Cellular Profiling of Compound 40. Having identified compound **40** with significantly improved murine pharmacokinetic performance and slightly improved affinity, we carried out functional assessments to ensure it remained on target and active in cells. Compound **40** was equally potent in our assay that monitors the transfer of a FAM-labeled NEDD8 to cullin substrates in a fully reconstituted NEDD8 cascade (IC_{50} = 0.11 μM, Figure S1),[16,29,37] demonstrating that the increased potency for blocking DCN1-UBE2M binding effectively translates to inhibition of neddylation. Importantly, compound **40**, and several other pyrazolo-pyridone analogues, showed a more rapid on-rate and slower dissociation rate than our original leads, demonstrating increased drug–target residence time compared to NAcM-OPT in surface plasmon resonance (SPR) assays (5- to 37-fold, Table S2 and S3). Slow dissociation of **40** suggests that the duration of occupancy of the intracellular DCN1–inhibitor complex is extended, which may boost efficacy and lengthen the duration of the effect.[38]

Having established the expected biochemical performance, we examined if the improvement in PK came at the expense of cellular potency. Compound **40** clearly maintains target engagement in a squamous cell carcinoma (SCC) cell line that contains DCN1 amplification (HCC95) as demonstrated with a cellular thermal shift assay (CETSA).[39] The DCN1 protein is

largely degraded at 52 °C in HCC95 cells treated with dimethyl sulfoxide (DMSO). However, in the presence of 10 μM of compound **40**, or the known DCN1/2 inhibitor NAcM-OPT,[15] the thermal stability of the DCN1 protein is clearly enhanced. Gratifyingly, it also appears that the improvement in biochemical potency and drug–target residence time translates to increased cellular target engagement a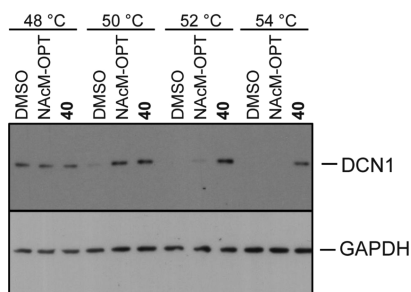s demonstrated by enhanced DCN1 stabilization in the CETSA assay (Figure 3) relative to NAcM-OPT. Dose–response experiments (Figure S4) suggest an approximate cellular EC$_{50}$ between 0.3 and 1 μM,

Figure 3. Enhancement of DCN1 thermal stability by compounds **40** and NAcM-OPT (positive control) but not by DMSO (negative control). HCC95 cells were treated with either DMSO or 10 μM of the indicated compound for 1 h, heated at the indicated temperature for 3 min, lysed, and blotted with the indicated antibodies.

relative to NAcM-OPT. Dose–response experiments (Figure S4) suggest an approximate cellular EC$_{50}$ between 0.3 and 1 μM, consistent with the biochemical IC$_{90}$ in the binding and functional assays.

Human DCN1 was originally discovered due to its over-expression in tumor cells, with amplification conferring anchorage-independent growth.[40] We have previously demonstrated that inhibitors of the DCN1 and UBE2M interaction restore anchorage dependency as scored in a soft-agar assay. Compound **40** inhibited colony formation completely at a concentration of 10 μM in this assay (Figure 4), showing that the
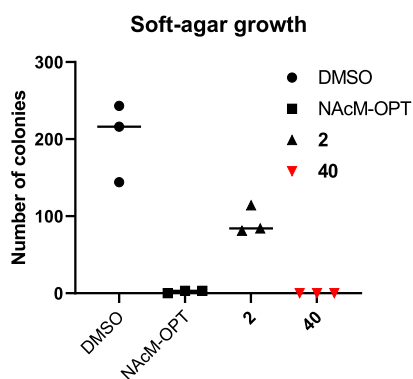

Figure 4. Soft-agar colony formation assay of DMSO, NAcM-OPT, **2**, and **40**. HCC95 cells were treated with either DMSO or 10 μM of the indicated compound. Colonies were counted at 10 days post-treatment. The experiment was repeated three times. Each data point is the average of colonies in three wells per one biological replicate.

expected phenotypic response is exhibited at concentrations where there is strong target engagement. Compound **40** is equally efficacious to NAcM-OPT at this concentration and significantly more efficacious than the early lead in the pyrazolo-pyridone series, compound **2**. Dose–response experiments (Figure S5) further support an approximate cellular EC$_{50}$ between 0.3 and 1 μM, consistent with the dose–response

CETSA assays (Figure S4). At this concentration, none of the compounds are growth inhibitory to HCC95 (EC$_{50}$ > 24 μM, data not shown). Additionally, none of the tested compounds inhibit the proliferation of normal fibroblasts (BJ; ATCC CRL-2522) up to the maximum tested concentration of 24 μM (data not shown).

■ DISCUSSION AND CONCLUSIONS

The overall goal of this study was to determine if this lead series could deliver potent inhibitors of the DCN1-UBE2M interaction that were also highly orally bioavailable and possessed reasonable to long in vivo half-life such that they were suitable for interrogating acute pharmacologic inhibition of DCN1/2-mediated cullin neddylation in murine models. Herein, we coupled a rational, structure-based design with empirical exploration of substituents to uncover the key structural elements critical for potency, solubility, and metabolic stability. The efficient synthetic routes outlined in Scheme 1 enabled rapid access to over 150 analogues to define the SAR/ SPR and permitted multi-gram-scale preparation of several key analogues. Ultimately, these studies identified compound **40**, which inhibits DCN1-UBE2M binding, blocks DCN1-mediated cullin neddylation, engages cellular DCN1 (Figure 3), and restores contact inhibition to HCC95 cells (Figure 4). Most importantly, **40** has a 25-fold improved plasma exposure, relative to compound **2**, and excellent oral bioavailability such that a single 50 mg/kg oral dose of **40** affords continuous murine plasma concentrations above its biochemical IC$_{90}$ (Figure 2) for 24 h.

This study had three major findings (Figure 5). First, the incorporation of a small hydrophobic ethyl substitution on the pyridone proved superior to hydrophilic substitutions and restored the activity of some of the *trans* diastereomers that had been previously universally inactive. Second, the methyl pyrazole affords access to an electronically and sterically tolerant primarily solvent-exposed subpocket. Substitution of the methyl pyrazole with ionizable polar substituents dramatically improved aqueous solubility without negatively affecting binding to the target or activity. Third, we established an in vitro–in vivo correlative model between microsomal stability and solubility and in vivo bioavailability that allowed us to confidently select optimized compounds for in vivo modeling. Metabolite identification studies after microsomal incubation focused our attention on the most rapidly metabolized moieties of the inhibitor series: the aryl ring targeting the hinge pocket. Electronic and steric deactivation of the aryl ring via the incorporation of the CF$_3$ substituent effectively suppressed oxidative metabolism in microsomal and murine models.

This new understanding of the determinants of bioavailability and potency led to the discovery of the optimized compound **40** that possesses greatly improved in vivo murine PK (oral bioavailability, C_{max}, IV Cl$_p$, and AUC) and strong effects in cellular assays. Improvement in inhibitory potency for the DCN1-UBE2M protein–protein interaction (TR-FRET) and drug–target residence time (SPR) translated well to inhibitory potency in preventing biochemical neddylation in the presence of the entire CRL complex (pulse-chase). In cellular models, compound **40** shows stronger thermal stabilization of the DCN1 protein relative to previous compounds, demonstrating that **40** effectively engages DCN1 in cells and that the alterations to its physiochemical properties did not significantly compromise permeability. Finally, compound **40** strongly inhibits anchorage-
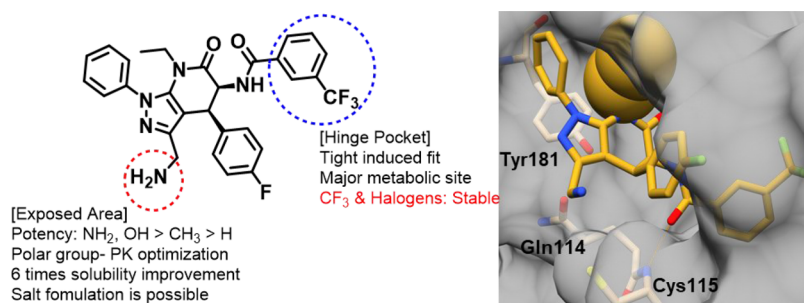
Figure 5. SAR, SPR summary, and X-ray crystal structure compound **40** bound to DCN1 (PDB ID: 7KWA).

independent colony formation of HCC95 cells, showing the primary expected phenotypic cellular response.

In conclusion, compound **40** is sufficiently potent and orally bioavailable to permit acute pharmacologic regulation of this highly complex and dynamic pathway in murine models. Ideally, this tool compound will enable the study of previously unappreciated biological roles of DCN1-mediated neddylation and provide further insights into DCN1/2's role in tumor progression. We are currently using compound **40** and others to dissect the effects of acute pharmacologic inhibition of the DCN1-UBE2M interaction on the NEDD8/CUL pathway in murine models and will report those results in due course.

■ EXPERIMENTAL SECTION

TR-FRET Assay. The TR-FRET assay was carried out in black 384-well microtiter plates (Corning 3573) at a final volume of 20 μL per well. The assay cocktail was prepared as a mixture of 50 nM biotin-DCN1, 20 nM Ac-UBE2M12-AlexaFluor 488, and 2.5 nM Tb streptavidin (Thermo Fisher) in assay buffer (25 mM HEPES, 100 mM NaCl, 0.1% Triton X-100, 0.5 mM DTT, pH 7.5). The assay cocktail was then incubated in bulk for 1 h at room temperature and then distributed (20 μL per well) using a WellMate instrument (Matrix). Compounds to be screened were added to assay plates from DMSO stock solutions by pin transfer using a pin tool (AFIX384FP1, V&P Scientific) adapted for manual transfer (BGPK, VP 381D-N, V&P Scientific) and equipped with 50SS pins (V&P Scientific). The assay plates were incubated for 1 h at room temperature prior to measuring the TR-FRET signal with a Clariostar plate reader (BMG Labtech) equipped with excitation maxima at 337 nm and emission maxima at 490 and 520 nm. We set the integration start to 100 μs and the integration time to 200 μs. The number of flashes was set to 100. The relative fluorescence ($E_x/E_m = 520{:}490$) was used for TR-FRET signal calculations. Assay end points were normalized from 0% (DMSO only) to 100% inhibition (unlabeled competitor peptide) for hit selection and curve fitting. All compounds were tested in triplicate or more.

Chemistry Experimental. *General.* All NMR data were collected at room temperature in CDCl$_3$ or (CD$_3$)$_2$SO on a 400 or 500 MHz Bruker or Agilent instrument. Solvents and reagents were used directly as obtained from commercial sources unless otherwise specified. Chemical shifts (δ) are reported in parts per million (ppm) with internal CHCl$_3$ (δ 7.26 ppm for ^{1}H and 77.0 ppm for ^{13}C), internal DMSO (δ 2.50 ppm for ^{1}H and 39.5 ppm for ^{13}C), or internal TMS (δ 0.0 ppm for ^{1}H and 0.0 ppm for ^{13}C) as the reference. ^{1}H NMR data are reported as follows: chemical shift, multiplicity (s = singlet, bs = broad singlet, d = doublet, t = triplet, q = quartet, p = pentet, sext = sextet, sep = septet, m = multiplet, dd = doublet of doublets, ddd = doublet of doublet of doublets, dt = doublet of triplets, td = triplet of doublets, tt = triplet of triplets, qd = quartet of doublets), coupling constant(s) (J) in Hertz (Hz), and integration. Flash column chromatography was performed using a Biotage Isolera One and Biotage KP-SIL SNAP cartridges. Purity was assessed by LC/MS/UV using a Waters Acquity UPLC-MS and by NMR spectroscopy. All compounds were confirmed to ≥95% purity prior to testing. Compounds that proved critical to our

SAR analysis were further characterized using ^{1}H NMR and HRMS/LRMS.

General Procedure. *A. Pyrazole Cyclization.* A solution of acetonitrile (1.5 mmol) in dry THF (2.0 mL) was cooled to −78 °C, and 2.5 M *n*-BuLi in hexanes (1.5 mmol) was added dropwise. The reaction mixture was stirred for 15 min at −78 °C, and ethyl 2-((*tert*-butyldimethylsilyl)oxy)acetate (1.0 mmol) was added. The reaction mixture was allowed to warm to ambient temperature and was stirred overnight. The reaction mixture was diluted with ice water. The residual aqueous mixture was acidified to pH = 5 and extracted with EtOAc. The combined organics were washed with brine, dried over MgSO$_4$, filtered, and concentrated.

To a solution of the intermediate in chlorobenzene (1.0 mL), hydrazine (1.0 mmol) was added and the reaction mixture was refluxed overnight. Upon cooling, the mixture was treated with saturated NaHCO$_3$ until basic and the mixture was extracted with CH$_2$Cl$_2$. The organic layer was dried over MgSO$_4$, filtered, and concentrated. The mixture was purified by flash chromatography.

B. Oxazolone Key Intermediate with Aliphatic Chain. B.1. Glycine Coupling. Carbonyl chloride (1.0 mmol) was added to a stirred solution of glycine (1.0 mmol) in 1 N aqueous sodium hydroxide (3.0 mL) dropwise. The reaction mixture was stirred at room temperature overnight. Then, the pH of the mixture was adjusted to 1−2 with 1 N aqueous HCl. The resulting solution was extracted with CH$_2$Cl$_2$, dried over MgSO$_4$, filtered, concentrated under reduced pressure, and purified by flash chromatography.

B.2. EDC Cyclization. Under a nitrogen atmosphere, the amine (1.0 mmol), EDCI·HCl (1.3 mmol), and DIPEA (1.3 mmol) were added to a solution of carboxylic acid (1.0 mmol) in CH$_2$Cl$_2$ (3 mL). The reaction mixture was stirred at room temperature overnight. The resulting solution was extracted with CH$_2$Cl$_2$, dried over MgSO$_4$, filtered, concentrated under reduced pressure, and purified by flash chromatography.

B.3. Al$_2$O$_3$ Condensation. Under a nitrogen atmosphere, the aldehyde (0.5 mmol) was added dropwise to a suspension of oxazolone (0.1 mmol), activated molecular sieves 4 Å (1.0 g), and activated aluminum oxide (1.0 mmol) in anhydrous CH$_2$Cl$_2$ (3 mL). The reaction mixture was stirred at room temperature for 6 h. The resulting solid was filtered through a pad of Celite to remove molecular sieves and Al$_2$O$_3$. The filtrate was dried under reduced pressure and then purified by flash chromatography.

C. Dihydropyridinone Cyclization. The reaction was performed under either condition (a) or (b).

(a) Under a nitrogen atmosphere, oxazolone (0.5 mmol) and tin (II) chloride (0.05 mmol) were added to a solution of amine (0.5 mmol) in chlorobenzene (1.0 mL). The reaction mixture was refluxed overnight. After cooling to room temperature, the mixture was extracted with EtOAc, washed with brine, dried over MgSO$_4$, filtered, concentrated under reduced pressure, and purified by flash chromatography.

(b) Under a nitrogen atmosphere, the oxazolone (0.5 mmol) was added to a solution of the amine (0.5 mmol) in chlorobenzene or *a,a,a*-trifluorotoluene (0.5 mL). The mixture was reacted at 150−180 °C in a sealed tube overnight. After cooling, the mixture was concentrated and the residue was precipitated in

hexane and filtered. Then, the crude product was purified by flash chromatography.

D. Dihydropyridinone-amide Substitution. D.1. Dihydropyridinone-amide Alkylation. Under a nitrogen atmosphere, cesium carbonate (1.1 mmol) and the alkyl halide (1.1 mmol) were added to a solution of dihydropyridinone (0.1 mmol) in DMF (1 mL). The reaction mixture was stirred overnight at room temperature or heated at 100 °C for 3 h. Then, the mixture was extracted with EtOAc, washed with brine, dried over MgSO$_4$, filtered, concentrated under reduced pressure, and purified by flash chromatography.

D.2. Dihydropyridinone-amide Acylation. Under a nitrogen atmosphere, pyridine (0.075 mmol) and acyl chloride (0.075 mmol) were added to a solution of dihydropyridinone (0.05 mmol) in CH$_2$Cl$_2$ (1.0 mL). The reaction mixture was stirred at room temperature overnight. Then, the mixture was extracted with EtOAc, washed with brine, dried over MgSO$_4$, filtered, concentrated under reduced pressure, and purified by flash chromatography.

E. Silyl Deprotection. To a solution of silyl-protected compound (1 mmol) in ACN (2 mL) under nitrogen atmosphere, 2 N HCl (3 mmol) was added and stirred at room temperature overnight. Then, the mixture was concentrated by reduced pressure, neutralized with sat. NaHCO$_3$ solution, extracted with CH$_2$Cl$_2$, washed with brine, dried with MgSO$_4$, filtered, and dried. The mixture was purified by flash chromatography.

F. Bromination (Appel Reaction). Carbon tetrabromide (1.7 mmol) was added portionwise to a solution of hydroxy compound (1.0 mmol) and triphenylphosphine (1.7 mmol) in CH$_2$Cl$_2$ (1 mL) that had been cooled to 0 °C and placed under nitrogen. The reaction was allowed to warm to rt and stirred for 2 h. The reaction mixture was filtered and washed with DCM. The filtrate was concentrated under reduced pressure. The crude product was purified by flash chromatography.

G. Gabriel Synthesis. To a solution of phthalimide (1.2 mmol) and potassium carbonate (1.2 mmol) in DMF (0.5 mL), bromo compound (1.0 mmol) in DMF (0.5 mL) was added at room temperature under nitrogen. The reaction was stirred overnight. The reaction mixture was extracted with EtOAc, washed by brine and water, dried over MgSO$_4$, and then filtered. The filtrate was concentrated under reduced pressure. The crude product was purified by flash chromatography.

To a solution of phthalimide-protected compound (1.0 mmol) in MeOH (1 mL) under nitrogen atmosphere, hydrazine monohydrate (3 mmol) was added and stirred at room temperature overnight. After concentrating and cooling, the mixture was filtered and washed by CH$_2$Cl$_2$ several times, and then the filtrate was purified by flash chromatography.

H. Amino Substitution. To a solution of bromo compound (1.0 mmol) in DCM (1.0 mL) under nitrogen atmosphere, amino compound (R$_1$R$_2$NH) (1.0 mmol) and DIPEA (1.1 mmol) were added and the reaction mixture was stirred at room temperature overnight. The mixture was extracted with CH$_2$Cl$_2$, washed with brine, dried with MgSO$_4$, filtered, and dried. Then, the crude product was purified by flash chromatography.

I. Acylation at Amino Group. To a solution of amino compound (1.0 mmol) in CH$_2$Cl$_2$ (1.0 mL) under nitrogen atmosphere at 0 °C, Ac$_2$O, MsCl, or R−COCl (1.0 mmol) and DIPEA (1.1 mmol) were added and the mixture was stirred at room temperature 1 h. The mixture was extracted with CH$_2$Cl$_2$, washed with brine, dried with MgSO$_4$, filtered, and dried. Then, the crude product was purified by flash chromatography.

J. Hydrolysis. To a solution of compound **4** (1.0 mmol) in 1,4-dioxane (10.0 mL) under nitrogen atmosphere, c-HCl (100 mmol) was added and refluxed overnight. The mixture was basified with 1 N NaOH, extracted with DCM, washed with brine, dried with MgSO$_4$, filtered, and dried. Then, the crude product was purified by flash chromatography.

K. Amide Coupling. The reaction was performed under either condition (a) or (b).

(a) To a solution of amine intermediate (1.0 mmol) in CH$_2$Cl$_2$ (1.0 mL), carboxylic acid (1.0 mmol), EDCI·HCl (1.3 mmol), and DIPEA (1.3 mmol) were added and stirred at room temperature

overnight. The mixture was extracted with EtOAc, washed with brine, dried with MgSO$_4$, filtered, and dried. Then, the crude product was purified by flash chromatography.

(b) To a solution of amine intermediate (1.0 mmol) in CH$_2$Cl$_2$ (1.0 mL), carbonyl chloride (1.0 mmol) and DIPEA (1.0 mmol) were added, and the mixture was stirred at room temperature for 3 h. The mixture was extracted with CH$_2$Cl$_2$, washed with brine, dried with MgSO$_4$, filtered, and dried. Then, the crude product was purified by flash chromatography.

Spectral Characterization of Key Compounds. *N-(rel-(4S,5S)-7-Ethyl-4-(4-fluorophenyl)-3-methyl-6-oxo-1-phenyl-4,5,6,7-tetrahydro-1H-pyrazolo[3,4-b]pyridin-5-yl)-3-methylbenzamide (Compound 2, Compound Characterization Agreed with Previous Reports).[33]* Compound **2** was synthesized by general procedures B−D starting from 4-fluorobenzaldehyde, (3-methylbenzoyl)glycine, and 3-methyl-1-phenyl-1H-pyrazol-5-amine.

^{1}H NMR (400 MHz, chloroform-*d*) δ 7.57 (s, 1H), 7.55−7.42 (m, 6H), 7.35−7.28 (m, 2H), 7.01−6.87 (m, 5H), 5.20 (dd, J = 7.1, 5.6 Hz, 1H), 4.77 (d, J = 7.0 Hz, 1H), 4.05−3.82 (m, 1H), 3.17 (dq, J = 14.0, 7.0 Hz, 1H), 2.39 (s, 3H), 2.14 (s, 3H), 0.99 (t, J = 7.1 Hz, 3H). ^{13}C NMR (101 MHz, chloroform-*d*) δ 168.0, 167.3, 161.0 (d, J = 246.8 Hz), 147.0, 139.1, 139.0, 138.6, 133.7, 132.7, 132.5, 132.4, 130.0, 129.9, 129.6 (2C), 128.8, 128.6, 127.7, 125.3, 124.1, 115.5, 115.3, 105.9, 55.7, 39.2, 36.7, 21.3, 12.7, 11.9. HRMS (ESI+) *m/z* calcd for C$_{29}$H$_{28}$FN$_4$O$_2^+$ [M + H]$^+$ 483.2191, found 483.2193.

N-(rel-(4S,5S)-7-Ethyl-4-(4-fluorophenyl)-3-methyl-6-oxo-1-phenyl-4,5,6,7-tetrahydro-1H-pyrazolo[3,4-b]pyridin-5-yl)-3-(trifluoromethyl)benzamide (Compound 4). Compound **4** was synthesized by general procedures B−D starting from 4-fluorobenzaldehyde, (3-(trifluoromethyl)benzoyl)glycine, and 3-methyl-1-phenyl-1H-pyrazol-5-amine.

^{1}H NMR (400 MHz, chloroform-*d*) δ 8.03 (s, 1H), 7.91−7.83 (m, 1H), 7.78 (d, J = 7.8 Hz, 1H), 7.57 (t, J = 7.8 Hz, 1H), 7.54−7.41 (m, 4H), 7.03 (d, J = 5.6 Hz, 1H), 6.96−6.88 (m, 4H), 5.20 (dd, J = 7.3, 5.7 Hz, 1H), 4.76 (d, J = 7.3 Hz, 1H), 3.97 (dq, J = 14.3, 7.2 Hz, 1H), 3.18 (dq, J = 14.0, 7.0 Hz, 1H), 2.15 (s, 3H), 1.00 (t, J = 7.0 Hz, 3H). ^{13}C NMR (126 MHz, chloroform-*d*) δ 170.3, 168.4, 165.0 (d, J = 247.0 Hz), 149.7, 141.8, 141.5, 137.3, 135.0 (2C), 134.0 (d, J = 33.2 Hz), 132.7, 132.5, 132.4, 132.3, 132.0, 131.6, 131.2 (q, J = 3.4 Hz), 128.0 (2C), 127.0 (q, J = 3.9 Hz), 126.3 (q, J = 272.4 Hz), 118.3, 118.1, 108.4, 58.5, 42.0, 39.4, 15.4, 14.6. HRMS (ESI+) *m/z* calcd for C$_{29}$H$_{25}$F$_4$N$_4$O$_2^+$ [M + H]$^+$ 537.1908, found 537.1917.

N-(rel-(4S,5S)-3-(Aminomethyl)-7-ethyl-4-(4-fluorophenyl)-6-oxo-1-phenyl-4,5,6,7-tetrahydro-1H-pyrazolo[3,4-b]pyridin-5-yl)-3-(trifluoromethyl)benzamide (Compound 40). Compound **40** was synthesized by general procedures A−F starting from 4-fluorobenzaldehyde, (3-(trifluoromethyl)benzoyl)glycine, and phenyl hydrazine.

^{1}H NMR (400 MHz, chloroform-*d*) δ 8.03 (s, 1H), 7.86 (d, J = 7.8 Hz, 1H), 7.80−7.76 (d, J = 7.8 Hz, 1H), 7.61−7.43 (m, 6H), 7.02 (d, J = 5.6 Hz, 1H), 6.99−6.88 (m, 4H), 5.23 (dd, J = 7.3, 5.6 Hz, 1H), 4.88 (d, J = 7.3 Hz, 1H), 3.97 (dq, J = 14.4, 7.2 Hz, 1H), 3.85−3.70 (m, 2H), 3.19 (dq, J = 13.9, 6.9 Hz, 1H), 1.00 (t, J = 7.1 Hz, 3H). ^{13}C NMR (101 MHz, chloroform-*d*) δ 167.7, 165.7, 162.4 (d, J = 247.2 Hz), 151.4, 139.2, 139.1, 134.5, 132.4 (2C), 131.4 (q, J = 32.9 Hz), 130.1, 129.8, 129.7, 129.6, 129.3, 129.1, 128.6 (q, J = 3.7 Hz), 125.4 (2C), 124.3 (q, J = 3.9 Hz), 122.2 (q, J = 275.4 Hz), 115.8, 115.6, 104.7, 55.8, 39.3, 38.7, 36.6, 12.7. HRMS (ESI+) *m/z* calcd for C$_{29}$H$_{26}$F$_4$N$_5$O$_2^+$ [M + H]$^+$ 552.2017, found 552.2028.

N-(rel-(4S,5S)-7-Ethyl-4-(4-fluorophenyl)-6-oxo-1-phenyl-3-(piperidin-1-ylmethyl)-4,5,6,7-tetrahydro-1H-pyrazolo[3,4-b]pyridin-5-yl)-3-(trifluoromethyl)benzamide (Compound 41). Compound **41** was synthesized by general procedures A−E and H starting from 4-fluorobenzaldehyde, (3-(trifluoromethyl)benzoyl)glycine, phenyl hydrazine, and piperidine.

^{1}H NMR (400 MHz, chloroform-*d*) δ 8.03 (s, 1H), 7.85 (d, J = 7.8 Hz, 1H), 7.77 (d, J = 7.7 Hz, 1H), 7.60−7.41 (m, 6H), 6.99−6.86 (m, 5H), 5.25−5.17 (m, 1H), 4.96 (d, J = 7.2 Hz, 1H), 3.94 (dq, J = 14.3, 7.2 Hz, 1H), 3.52 (d, J = 13.8 Hz, 1H), 3.31 (d, J = 13.7 Hz, 1H), 3.21 (dq, J = 14.0, 6.9 Hz, 1H), 2.34−2.10 (m, 4H), 1.33−1.18 (m, 4H), 1.13−1.04 (m, 2H), 1.01 (t, J = 7.1 Hz, 3H). ^{13}C NMR (126 MHz,

chloroform-d) δ 170.7, 168.4, 164.9 (d, J = 246.1 Hz), 151.5, 147.6, 141.9, 141.8, 137.5, 135.8 (q, J = 3.7 Hz), 134.0 (q, J = 33.4 Hz), 132.7, 132.5, 132.4, 132.2, 132.0, 131.7, 131.1 (d, J = 3.8 Hz), 128.4 (q, J = 273.5 Hz), 128.2 (2C), 127.0 (q, J = 3.8 Hz), 118.0, 117.9, 108.9, 58.8, 58.5 (2C), 57.3, 42.1, 39.7, 28.1 (2C), 26.7, 15.4. HRMS (ESI+) m/z calcd for $C_{34}H_{34}F_4N_5O_2^+$ [M + H]⁺ 620.2643, found 620.2637.

N-(rel-(4R,5S)-7-Ethyl-4-(4-fluorophenyl)-3-methyl-6-oxo-1-phenyl-4,5,6,7-tetrahydro-1H-pyrazolo[3,4-b]pyridin-5-yl)-3-(trifluoromethyl)benzamide (Compound 125). Compound **125** was synthesized by general procedures B−D starting from 4-fluorobenzaldehyde, (3-(trifluoromethyl)benzoyl)glycine, and 3-methyl-1-phenyl-1H-pyrazol-5-amine.

¹H NMR (500 MHz, chloroform-d) δ 7.88 (s, 1H), 7.81 (d, J = 7.9 Hz, 1H), 7.73 (d, 1H), 7.57−7.51 (m, 2H), 7.51−7.44 (m, 4H), 7.44−7.32 (m, 3H), 7.08−7.02 (m, 2H), 6.53 (d, J = 9.0 Hz, 1H), 5.44 (dd, J = 12.8, 9.0 Hz, 1H), 4.12 (d, J = 12.8 Hz, 1H), 3.93 (dq, J = 14.3, 7.1 Hz, 1H), 3.17 (dq, J = 13.9, 6.9 Hz, 1H), 1.60 (s, 3H), 0.92 (t, J = 7.0 Hz, 3H). ¹³C NMR (101 MHz, chloroform-d) δ 169.5, 166.3, 162.3 (q, J = 247.1 Hz), 146.4, 139.0, 138.3, 134.5, 132.7, 132.7, 131.1 (q, J = 32.8 Hz), 130.5, 130.4, 130.2, 129.5, 129.1, 128.8, 128.3 (q, J = 3.5 Hz), 126.3 (q, J = 273.6 Hz), 125.0 (2C), 124.0 (q, J = 4.0 Hz), 115.8, 115.6, 106.4, 56.3, 42.9, 39.4, 13.0, 12.9. HRMS (ESI+) m/z calcd for $C_{29}H_{25}F_4N_4O_2^+$ [M + H]⁺ 537.1908, found 537.1896.

N-(rel-(4S,5S)-3-(Aminomethyl)-7-ethyl-4-(6-fluoropyridin-3-yl)-6-oxo-1-phenyl-4,5,6,7-tetrahydro-1H-pyrazolo[3,4-b]pyridin-5-yl)-3-(trifluoromethyl)benzamide (Compound 143). Compound **143** was synthesized by general procedures A−F starting from 6-fluoronicotinaldehyde, (3-(trifluoromethyl)benzoyl)glycine, and phenyl hydrazine.

¹H NMR (400 MHz, chloroform-d) δ 8.07 (s, 1H), 7.89 (d, J = 7.9 Hz, 1H), 7.87−7.84 (m, 1H), 7.80 (d, J = 7.7 Hz, 1H), 7.63−7.45 (m, 6H), 7.39 (td, J = 8.0, 2.5 Hz, 1H), 7.17 (d, J = 4.9 Hz, 1H), 6.81 (dd, J = 8.4, 2.9 Hz, 1H), 5.22 (dd, J = 7.1, 4.9 Hz, 1H), 5.04 (d, J = 7.2 Hz, 1H), 3.98 (dq, J = 14.3, 7.2 Hz, 1H), 3.88−3.73 (m, 2H), 3.17 (dt, J = 13.8, 7.0 Hz, 1H), 0.99 (t, J = 7.1 Hz, 3H). ¹³C NMR (101 MHz, chloroform-d) δ 167.2, 165.8, 163.2 (d, J = 240.3 Hz), 147.5, 147.3, 141.0, 140.9, 139.1, 138.9, 134.1, 131.5 (q, J = 32.8 Hz), 130.0, 129.7, 129.4, 129.3, 128.8 (q, J = 3.1 Hz), 125.5 (2C), 124.4 (q, J = 4.0 Hz), 123.6 (q, J = 273.0 Hz), 109.7, 109.4, 103.6, 55.7, 39.3, 38.7, 34.1, 12.8. HRMS (ESI+) m/z calcd for $C_{28}H_{25}F_4N_6O_2^+$ [M + H]⁺ 553.1970, found 553.1967.

ASSOCIATED CONTENT

ⓢ Supporting Information

The Supporting Information is available free of charge at https://pubs.acs.org/doi/10.1021/acs.jmedchem.1c00035.

> Characterization details for the other synthetic compounds as well as additional information from X-ray crystallography and biological studies; chemical characterization and purity data; expanded SAR tables including all compounds; pulse chase data for compound **40**; surface plasmon resonance (SPR) data; metabolite identification studies for compound **2**; in vivo PK data; data collection and refinement statistics for lysozyme-DCN1P:**1** and Lysozyme-DCN1P:**40** (PDF)

> Molecular formula strings and TR-FRET potency (CSV)

Accession Codes

Atomic coordinates and experimental data for the X-ray co-crystal structures of NAcM-OPT (PDB: 5V86) and **40** (PDB: 7KWA) in complex with lysozyme−DCN1ᴾ are available from the RCSB Protein Data Bank (www.rcsb.org). The authors will release the atomic coordinates and experimental data upon article publication.

AUTHOR INFORMATION

Corresponding Author

R. Kiplin Guy − *Department of Pharmaceutical Sciences, University of Kentucky, Lexington, Kentucky 40508, United States;* ⓞ orcid.org/0000-0002-9638-2060; Phone: (859) 257-5290; Email: kip.guy@uky.edu; Fax: (859) 257-2128

Authors

Ho Shin Kim − *Department of Pharmaceutical Sciences, University of Kentucky, Lexington, Kentucky 40508, United States*

Jared T. Hammill − *Department of Pharmaceutical Sciences, University of Kentucky, Lexington, Kentucky 40508, United States*

Daniel C. Scott − *Department of Structural Biology, St. Jude Children's Research Hospital, Memphis, Tennessee 38105, United States*

Yizhe Chen − *Department of Pharmaceutical Sciences, University of Kentucky, Lexington, Kentucky 40508, United States*

Amy L. Rice − *Department of Pharmaceutical Sciences, University of Kentucky, Lexington, Kentucky 40508, United States*

William Pistel − *Department of Pharmaceutical Sciences, University of Kentucky, Lexington, Kentucky 40508, United States*

Bhuvanesh Singh − *Department of Surgery, Laboratory of Epithelial Cancer Biology, Memorial Sloan Kettering Cancer Center, New York 10065, United States*

Brenda A. Schulman − *Department of Structural Biology, St. Jude Children's Research Hospital, Memphis, Tennessee 38105, United States; Department of Molecular Machines and Signaling, Max Planck Institute of Biochemistry, Martinsried 82152, Germany*

Complete contact information is available at:
https://pubs.acs.org/10.1021/acs.jmedchem.1c00035

Author Contributions

The manuscript was written through contributions of all authors. All authors have given approval to the final version of the manuscript.

Notes

The authors declare the following competing financial interest(s): Inventors on United States Patent Application 20180256558, METHODS AND COMPOSITIONS OF INHIBITING DCN1-UBC12 INTERACTION and United States Patent 10,525,048, Methods and compositions of inhibiting DCN1-UBC12 interaction. BAS is a member of the Scientific Advisory Board of Interline Therapeutics.

thank the staff at the ALS 8.2.1 and Sercat 22-ID beamlines at the Advanced Light Source and Advanced Photon Source.

ABBREVIATIONS

DCN1, defective in cullin neddylation 1; UBL, ubiquitin-like protein; UBE2M, NEDD8-conjugating enzyme Ubc12; SCCRO, squamous cell carcinoma-related oncogene; SCC, squamous cell carcinoma; CRL, cullin-RING ligases; NEDD8, Neural precursor cell expressed, developmentally downregulated 8; SAR, structure–activity relationship; SPR, structure–property relationship; TR-FRET, time-resolved fluorescence resonance energy transfer; HTS, high-throughput screen; *t*-Bu, *tert*-butyl; CETSA, cellular thermal shift assay; ROS, reactive oxygen species; NAE, NEDD8-activating enzyme; RBX1, Ring-Box 1, E3 Ubiquitin Protein Ligase; CUL1, cullin 1; AF, AlexaFluor 488

REFERENCES

(1) Petroski, M. D.; Deshaies, R. J. Function and regulation of cullin-RING ubiquitin ligases. *Nat. Rev. Mol. Cell Biol.* **2005**, *6*, 9−20.

(2) Lu, A.; Pfeffer, S. R. A CULLINary ride across the secretory pathway: more than just secretion. *Trends Cell Biol.* **2014**, *24*, 389−399.

(3) Cui, D.; Xiong, X.; Zhao, Y. Cullin-RING ligases in regulation of autophagy. *Cell Div.* **2016**, *11*, No. 8.

(4) Bielskienė, K.; Bagdoniene, L.; Mozuraitiene, J.; Kazbariene, B.; Janulionis, E. E3 ubiquitin ligases as drug targets and prognostic biomarkers in melanoma. *Medicina* **2015**, *51*, 1−9.

(5) Bulatov, E.; Ciulli, A. Targeting Cullin-RING E3 ubiquitin ligases for drug discovery: structure, assembly and small-molecule modulation. *Biochem. J.* **2015**, *467*, 365−386.

(6) Huang, X.; Dixit, V. M. Drugging the undruggables: exploring the ubiquitin system for drug development. *Cell Res.* **2016**, *26*, 484−498.

(7) Weathington, N. M.; Mallampalli, R. K. Emerging therapies targeting the ubiquitin proteasome system in cancer. *J. Clin. Invest.* **2014**, *124*, 6−12.

(8) Yu, Q.; Jiang, Y.; Sun, Y. Anticancer drug discovery by targeting cullin neddylation. *Acta Pharm. Sin. B* **2020**, *10*, 746−765.

(9) Becker, T.; Le-Trilling, V. T. K.; Trilling, M. Cellular Cullin RING Ubiquitin Ligases: Druggable Host Dependency Factors of Cytomegaloviruses. *Int. J. Mol. Sci.* **2019**, *20*, No. 1636.

(10) Wu, K.; Chong, R. A.; Yu, Q.; Bai, J.; Spratt, D. E.; Ching, K.; Lee, C.; Miao, H.; Tappin, I.; Hurwitz, J.; Zheng, N.; Shaw, G. S.; Sun, Y.; Felsenfeld, D. P.; Sanchez, R.; Zheng, J. N.; Pan, Z. Q. Suramin inhibits cullin-RING E3 ubiquitin ligases. *Proc. Natl. Acad. Sci. U.S.A.* **2016**, *113*, E2011−E2018.

(11) Zhang, X.; Shi, S.; Su, Y.; Yang, X.; He, S.; Yang, X.; Wu, J.; Zhang, J.; Rao, F. Suramin and NF449 are IP5K inhibitors that disrupt inositol hexakisphosphate-mediated regulation of cullin-RING ligase and sensitize cancer cells to MLN4924/pevonedistat. *J. Biol. Chem.* **2020**, *295*, 10281−10292.

(12) Clinical Trials Using Pevonedistat . https://www.cancer.gov/about-cancer/treatment/clinical-trials/intervention/pevonedistat (accessed: 4/8/2021).

(13) Schlierf, A.; Altmann, E.; Quancard, J.; Jefferson, A. B.; Assenberg, R.; Renatus, M.; Jones, M.; Hassiepen, U.; Schaefer, M.; Kiffe, M.; Weiss, A.; Wiesmann, C.; Sedrani, R.; Eder, J.; Martoglio, B. Targeted inhibition of the COP9 signalosome for treatment of cancer. *Nat. Commun.* **2016**, *7*, No. 13166.

(14) Abidi, N.; Xirodimas, D. P. Regulation of cancer-related pathways by protein NEDDylation and strategies for the use of NEDD8 inhibitors in the clinic. *Endocr.-Relat. Cancer* **2015**, *22*, T55−T70.

(15) Scott, D. C.; Hammill, J. T.; Min, J.; Rhee, D. Y.; Connelly, M.; Sviderskiy, V. O.; Bhasin, D.; Chen, Y.; Ong, S. S.; Chai, S. C.; Goktug, A. N.; Huang, G.; Monda, J. K.; Low, J.; Kim, H. S.; Paulo, J. A.; Cannon, J. R.; Shelat, A. A.; Chen, T.; Kelsall, I. R.; Alpi, A. F.; Pagala, V.; Wang, X.; Peng, J.; Singh, B.; Harper, J. W.; Schulman, B. A.; Guy, R.

K. Blocking an N-terminal acetylation-dependent protein interaction inhibits an E3 ligase. *Nat. Chem. Biol.* **2017**, *13*, 850−857.

(16) Scott, D. C.; Sviderskiy, V. O.; Monda, J. K.; Lydeard, J. R.; Cho, S. E.; Harper, J. W.; Schulman, B. A. Structure of a RING E3 trapped in action reveals ligation mechanism for the ubiquitin-like protein NEDD8. *Cell* **2014**, *157*, 1671−1684.

(17) Keuss, M. J.; Thomas, Y.; McArthur, R.; Wood, N. T.; Knebel, A.; Kurz, T. Characterization of the mammalian family of DCN-type NEDD8 E3 ligases. *J. Cell Sci.* **2016**, *129*, 1441−1454.

(18) Zhang, Z. H.; Li, J.; Luo, F.; Wang, Y. S. Clinical significance of SCCRO (DCUN1D1) in prostate cancer and its proliferation-inhibiting effect on Lncap cells. *Eur. Rev. Med. Pharmacol. Sci.* **2017**, *21*, 4283−4291.

(19) Kurz, T.; Chou, Y. C.; Willems, A. R.; Meyer-Schaller, N.; Hecht, M. L.; Tyers, M.; Peter, M.; Sicheri, F. Dcn1 functions as a scaffold-type E3 ligase for cullin neddylation. *Mol. Cell* **2008**, *29*, 23−35.

(20) Kurz, T.; Ozlu, N.; Rudolf, F.; O'Rourke, S. M.; Luke, B.; Hofmann, K.; Hyman, A. A.; Bowerman, B.; Peter, M. The conserved protein DCN-1/Dcn1p is required for cullin neddylation in C. elegans and S. cerevisiae. *Nature* **2005**, *435*, 1257−1261.

(21) Cao, B.; Wang, Y.; Wen, D.; Liu, W.; Wang, J.; Fan, G.; Ruan, L.; Song, B.; Cai, Y.; Wei, M.; Li, X.; Xia, J.; Chen, N.; Xiang, J.; Yu, T.; Bai, T.; Xie, X.; Zhang, L.; Li, C.; Yuan, Y.; Chen, H.; Li, H.; Huang, H.; Tu, S.; Gong, F.; Liu, Y.; Wei, Y.; Dong, C.; Zhou, F.; Gu, X.; Xu, J.; Liu, Z.; Zhang, Y.; Li, H.; Shang, L.; Wang, K.; Li, K.; Zhou, X.; Dong, X.; Qu, Z.; Lu, S.; Hu, X.; Ruan, S.; Luo, S.; Wu, J.; Peng, L.; Cheng, F.; Pan, L.; Zou, J.; Jia, C.; Wang, J.; Liu, X.; Wang, S.; Wu, X.; Ge, Q.; He, J.; Zhan, H.; Qiu, F.; Guo, L.; Huang, C.; Jaki, T.; Hayden, F. G.; Horby, P. W.; Zhang, D.; Wang, C. A Trial of Lopinavir-Ritonavir in Adults Hospitalized with Severe Covid-19. *N. Engl. J. Med.* **2020**, *382*, 1787−1799.

(22) Huang, G.; Kaufman, A. J.; Xu, K.; Manova, K.; Singh, B. Squamous cell carcinoma-related oncogene (SCCRO) neddylates Cul3 protein to selectively promote midbody localization and activity of Cul3KLHL21 protein complex during abscission. *J. Biol. Chem.* **2017**, *292*, 15254−15265.

(23) Fu, W.; Sun, J.; Huang, G.; Liu, J. C.; Kaufman, A.; Ryan, R. J.; Ramanathan, S. Y.; Venkatesh, T.; Singh, B. Squamous Cell Carcinoma Related Oncogene (SCCRO) Family Members Regulate Cell Growth and Proliferation through Their Cooperative and Antagonistic Effects on Cullin Neddylation. *J. Biol. Chem.* **2016**, *291*, 6200−6217.

(24) Sarkaria, I.; Pornchai, O.; Talbot, S. G.; Reddy, P. G.; Ngai, I.; Maghami, E.; Patel, K. N.; Lee, B.; Yonekawa, Y.; Dudas, M.; Kaufman, A.; Ryan, R.; Ghossein, R.; Rao, P. H.; Stoffel, A.; Ramanathan, Y.; Singh, B. Squamous cell carcinoma related oncogene/DCUN1D1 is highly conserved and activated by amplification in squamous cell carcinomas. *Cancer Res.* **2006**, *66*, 9437−9444.

(25) Scott, D. C.; Monda, J. K.; Bennett, E. J.; Harper, J. W.; Schulman, B. A. N-terminal acetylation acts as an avidity enhancer within an interconnected multiprotein complex. *Science* **2011**, *334*, 674−678.

(26) Monda, J. K.; Scott, D. C.; Miller, D. J.; Lydeard, J.; King, D.; Harper, J. W.; Bennett, E. J.; Schulman, B. A. Structural conservation of distinctive N-terminal acetylation-dependent interactions across a family of mammalian NEDD8 ligation enzymes. *Structure* **2013**, *21*, 42−53.

(27) Hammill, J. T.; Bhasin, D.; Scott, D. C.; Min, J.; Chen, Y.; Lu, Y.; Yang, L.; Kim, H. S.; Connelly, M. C.; Hammill, C.; Holbrook, G.; Jeffries, C.; Singh, B.; Schulman, B. A.; Guy, R. K. Discovery of an Orally Bioavailable Inhibitor of Defective in Cullin Neddylation 1 (DCN1)-Mediated Cullin Neddylation. *J. Med. Chem.* **2018**, *61*, 2694−2706.

(28) Hammill, J. T.; Scott, D. C.; Min, J.; Connelly, M. C.; Holbrook, G.; Zhu, F.; Matheny, A.; Yang, L.; Singh, B.; Schulman, B. A.; Guy, R. K. Piperidinyl Ureas Chemically Control Defective in Cullin Neddylation 1 (DCN1)-Mediated Cullin Neddylation. *J. Med. Chem.* **2018**, *61*, 2680−2693.

(29) Scott, D. C.; Hammill, J. T.; Min, J.; Rhee, D. Y.; Connelly, M.; Sviderskiy, V. O.; Bhasin, D.; Chen, Y.; Ong, S.-S.; Chai, S. C.; et al.

Blocking an N-terminal acetylation-dependent protein interaction inhibits an E3 ligase. *Nat. Chem. Biol.* **2017**, *13*, 850−857.

(30) Zhou, H.; Lu, J.; Liu, L.; Bernard, D.; Yang, C. Y.; Fernandez-Salas, E.; Chinnaswamy, K.; Layton, S.; Stuckey, J.; Yu, Q.; Zhou, W.; Pan, Z.; Sun, Y.; Wang, S. A potent small-molecule inhibitor of the DCN1-UBC12 interaction that selectively blocks cullin 3 neddylation. *Nat. Commun.* **2017**, *8*, No. 1150.

(31) Zhou, H.; Zhou, W.; Zhou, B.; Liu, L.; Chern, T. R.; Chinnaswamy, K.; Lu, J.; Bernard, D.; Yang, C. Y.; Li, S.; Wang, M.; Stuckey, J.; Sun, Y.; Wang, S. High-Affinity Peptidomimetic Inhibitors of the DCN1-UBC12 Protein−Protein Interaction. *J. Med. Chem.* **2018**, *61*, 1934−1950.

(32) Wang, S.; Zhao, L.; Shi, X.-J.; Ding, L.; Yang, L.; Wang, Z.-Z.; Shen, D.; Tang, K.; Li, X.-J.; Mamun, M. A. A.; Li, H.; Yu, B.; Zheng, Y.-C.; Wang, S.; Liu, H.-M. Development of Highly Potent, Selective, and Cellular Active Triazolo[1,5-a]pyrimidine-Based Inhibitors Targeting the DCN1−UBC12 Protein−Protein Interaction. *J. Med. Chem.* **2019**, *62*, 2772−2797.

(33) Kim, H. S.; Hammill, J. T.; Scott, D. C.; Chen, Y.; Min, J.; Rector, J.; Singh, B.; Schulman, B. A.; Guy, R. K. Discovery of Novel Pyrazolopyridone DCN1 Inhibitors Controlling Cullin Neddylation. *J. Med. Chem.* **2019**, *62*, 8429−8442.

(34) Izumi, S.; Kobayashi, Y.; Takemoto, Y. Catalytic Asymmetric Synthesis of anti-alpha,beta-Diamino Acid Derivatives. *Org. Lett.* **2016**, *18*, 696−699.

(35) Shi, F.; Zhang, J.; Tu, S.; Jia, R.; Zhang, Y.; Jiang, B.; Jiang, H. An efficient synthesis of new class of pyrazolo [3, 4-b] pyridine-6-one derivatives by a novel cascade reaction. *J. Heterocycl. Chem.* **2007**, *44*, 1013−1017.

(36) Ritchie, T. J.; Macdonald, S. J. The impact of aromatic ring count on compound developability–are too many aromatic rings a liability in drug design? *Drug Discovery Today* **2009**, *14*, 1011−1020.

(37) Scott, D. C.; Monda, J. K.; Bennett, E. J.; Harper, J. W.; Schulman, B. A. N-terminal acetylation acts as an avidity enhancer within an interconnected multiprotein complex. *Science* **2011**, *334*, 674−678.

(38) Copeland, R. A.; Pompliano, D. L.; Meek, T. D. Drug-target residence time and its implications for lead optimization. *Nat. Rev. Drug Discovery* **2006**, *5*, 730−739.

(39) Molina, D. M.; Jafari, R.; Ignatushchenko, M.; Seki, T.; Larsson, E. A.; Dan, C.; Sreekumar, L.; Cao, Y.; Nordlund, P. Monitoring drug target engagement in cells and tissues using the cellular thermal shift assay. *Science* **2013**, *341*, 84−87.

(40) Sarkaria, I.; Pornchai, O.; Talbot, S. G.; Reddy, P. G.; Ngai, I.; Maghami, E.; Patel, K. N.; Lee, B.; Yonekawa, Y.; Dudas, M.; Kaufman, A.; Ryan, R.; Ghossein, R.; Rao, P. H.; Stoffel, A.; Ramanathan, Y.; Singh, B. Squamous cell carcinoma related oncogene/DCUN1D1 is highly conserved and activated by amplification in squamous cell carcinomas. *Cancer Res.* **2006**, *66*, 9437−9444.